



AIAA 2000-2475

## Rotorcraft Retreating Blade Stall Control

P. Lorber, D. McCormick, T. Anderson, B. Wake, and D. MacMartin  
United Technologies Research Center  
East Hartford CT

M. Pollack  
Sikorsky Aircraft Corporation  
Stratford, CT

T. Corke  
University of Notre Dame  
Notre Dame, IN

K. Breuer  
Brown University  
Providence, RI

**FLUIDS 2000 Conference and Exhibit**

19-22 June 2000  
Denver Colorado

# ROTORCRAFT RETREATING BLADE STALL CONTROL

Peter F. Lorber, Duane C. McCormick, Torger J. Anderson,  
Brian E. Wake, and Douglas G. MacMartin  
United Technologies Research Center  
East Hartford CT

Michael J. Pollack  
Sikorsky Aircraft Corporation  
Stratford, CT

Thomas C. Corke  
University of Notre Dame  
Notre Dame, IN

Kenneth Breuer  
Brown University  
Providence, RI

## Abstract

Flow control to avoid or delay rotorcraft retreating blade stall can be an enabling technology for future high performance rotorcraft. Aerodynamic experiments and computations have indicated that appropriate unsteady excitation can delay boundary layer separation and stall on airfoils. Work is in progress to determine the control requirements for helicopter rotor blades at full scale Mach numbers, Reynolds numbers, and with unsteady pitching motions. Compact, powerful, and efficient flow actuation and control systems will be needed. Three actuation concepts were favorably evaluated during initial studies: electromechanical directed synthetic jets (DSJ), periodic flow modulation, and plasma actuation. Electromechanical DSJ and plasma actuators are being developed further and will be evaluated in full scale pitching blade section experiments. These experiments will determine the required control authority, validate the actuator concepts, and study open and closed loop control approaches. Computational studies are being performed of the combined external and actuator flow fields to determine preferred actuation geometries and operating points. System analyses are being used to quantify the benefits for representative aircraft configurations and missions.

---

Copyright ©2000 by United Technologies Corporation. Published by the American Institute of Aeronautics and Astronautics, Inc., with Permission.

## Nomenclature

$A$	airfoil pitch rate, $\dot{\alpha}c / 2U$
$c$	airfoil chord
$C_L$	section lift coefficient, $L / 0.5\rho cU^2$
$C_\mu$	momentum coefficient, $(\rho hu^2)_{JET} / (\rho cU^2)_\infty$
$F_+$	jet frequency, $f_{JET}c/U$
$h$	jet slot width
$k$	reduced frequency, $\omega c / 2U$
$M$	freestream Mach number
$Re$	Reynolds number, $Uc / \nu$
$u_{JET}$	jet unsteady velocity amplitude
$U$	freestream velocity

## Introduction

High performance future rotorcraft will require significant improvements in multiple attributes, including increased range for global self-deployability, increased speed and performance for fast, agile missions, increased payload, and reduced external noise emissions, cabin noise and vibration. Analyses such as the Rotary Wing Vehicle Technology Development Approach (TDA) and the Army After Next (AAN) have defined specific objectives for military vehicles. One set of relevant objectives includes:

- 24% increase in blade loading
- 20% reduction in drag
- 10% increase in aerodynamic efficiency
- 112% increase in maneuverability/agility
- 60% reduction in vibratory loads

Substantial improvements such as these will also be required to expand the use of civilian rotorcraft beyond current applications. Since traditional passive designs appear incapable of producing sufficiently large simultaneous improvements in these attributes, active systems for controlling rotor loads, performance, and acoustics are being extensively studied. (Refs. 1-5).

Active flow control technologies can play a significant role by providing the means to avoid or delay retreating blade stall. Retreating Blade Stall (RBS) establishes limits on rotor load and flight speed. In addition to the loss of capability to generate lift, unsteady blade stall transmits very large impulsive blade pitching moments to the flight control system. In order to prevent excess control loads, a stall boundary must be set to define the maximum blade load capability as a function of rotor load and flight speed. These limits impact maneuverability and agility as well as speed and payload.

The fluid mechanism involved in blade stall is boundary layer separation near the leading edge of the rotor blade during rapid motion to high blade angle of attack. This dynamic stall phenomenon has been extensively studied using pitching airfoil and three dimensional blade sections at both model and full scale (Refs. 6-8, Fig. 1) and by computations (Ref. 9-11). At full scale, reduced frequencies are typically  $k \sim 0.05$  to  $0.15$ , with maximum instantaneous pitch rates of  $A \sim 0.002$  to  $0.02$ . The relative external flow Mach numbers are  $M = 0.3 - 0.5$ , while the peak local Mach numbers near the separation location of  $x/c = 0.05$  to  $0.15$  are typically  $M = 1.1$  to  $1.3$ . Full scale Reynolds numbers are  $Re \sim 4 \times 10^6$ , with transition to turbulence occurring ahead of separation.

Stalled flow locations on the rotor disc have been identified by surface pressure measurements during flight test of a full scale aircraft (Ref. 12, Fig. 2), and by surface pressure, heat transfer, and tuft measurements during wind tunnel test of model rotors (Ref. 13, Fig. 3). Figure 4 is based on model rotor experimental data for a level flight condition, and shows the relatively small stall regions for a moderate load condition, and significantly larger stall regions at a high load condition that is very close to the stall boundary. Figure 5 show similar stall patterns obtained from blade pressure measurements on a maneuvering aircraft (Ref. 12). The combination of detailed unsteady airfoil experiments and computations and global rotor measurements has defined the RBS phenomenon that must be controlled and the conditions under which the control is required.

A practical way of avoiding or significantly delaying RBS has not yet been demonstrated under

flight conditions. Separation control must mitigate the effects of the dynamic stall vorticity on blade pitching



Figure 1. Full scale pitching 3D rotor blade model used for dynamic stall investigations (Ref. 8).



Figure 2. Black Hawk aircraft used for pressure instrumented rotor measurements of stall (Ref.12).

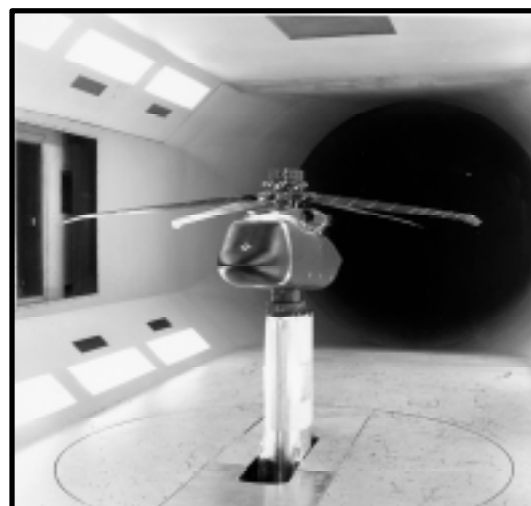


Figure 3. Pressure instrumented model rotor used for stall boundary investigations (Ref 13.).

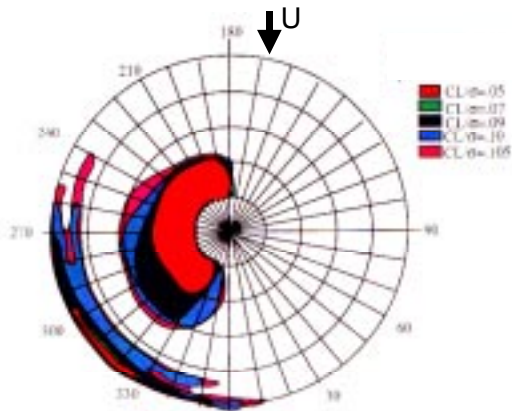


Figure 4. Measured blade stall regions from model rotor for level flight at increasing rotor thrust (Ref. 13).

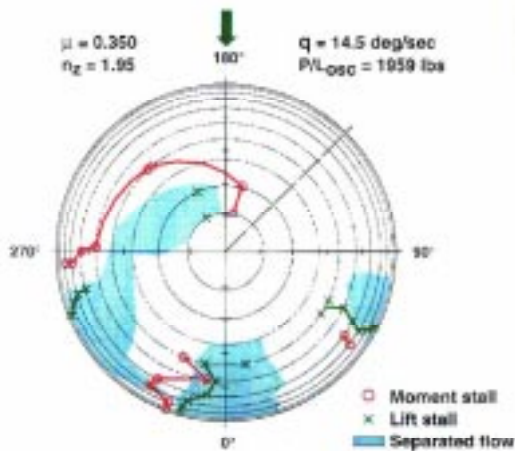


Figure 5. Stall regions identified from maneuvering aircraft blade pressure measurements (Ref. 12).

moment, and maintain or increase the available lift. This must be accomplished in an unsteady, compressible, high Reynolds number flow. The stall control approach that is applied on the retreating blade side must not create a significant drag penalty on the advancing side, where the relative external Mach numbers are 0.6 to 0.85. Further, the approach must be practically incorporated into a rotating blade.

Mechanical high lift devices such as leading edge slats have been investigated and found to be able to delay dynamic stall (Refs. 14-15), but published designs have tended to either create excess drag if left in place on the advancing side or to be impractical to deploy and retract each rotor revolution. Steady flow control methods such as air injection (Ref. 16) or suction (Ref. 17) have also been investigated, but transferring sufficient fluid from the fixed to rotating systems at acceptable levels of power and complexity

presents significant difficulties. Successful application of flow control to the rotor blade will require the development of new and innovative technologies that integrate a thorough understanding of the underlying fluid dynamics with a robust and efficient actuation, sensing, and control system.

This paper presents results from a study of flow control alternatives for RBS control, identifies some of the expected aircraft system benefits, and describes the approaches currently being pursued to develop and validate practical RBS control as part of the Defense Advanced Research Projects Agency (DARPA) MicroAdaptive Flow Control (MAFC) program.

### Flow Control Technologies

Unsteady excitation has frequently been investigated as a way to delay or avoid separation (Ref. 18). An extensive series of recent experiments were conducted by Wygnanski and his current and former students (Refs. 19-21). While the precise mechanism is not fully understood, the concept involves low level periodic forcing to modulate the formation of vortices in a separating flow. At or near an optimum frequency of  $F^+ \sim 1$ , high streamwise momentum flow is driven towards the surface, energizing the boundary layer and avoiding massive separation (Fig. 6). The periodic excitation has been provided by moving a mechanical element, by injecting an unsteady jet of air, or by alternate suction and blowing. For the later two methods, the key parameter is the momentum coefficient,  $C_{\mu}$ . While a substantial quantity of work has been presented, definitive results for rotor blades at full scale flight conditions are not yet available.

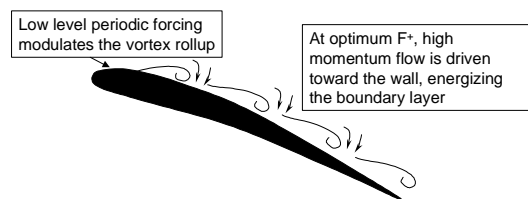


Figure 6. Periodic excitation concept for separation control.

The primary separation control technique being applied in the current work is the Directed Synthetic Jet (DSJ). It applies acoustic streaming (Ref. 22) to form a synthetic jet (Ref. 23) with an exit neck optimized for separation control (Ref. 24). Figure 7 shows a typical DSJ configuration. The curved neck allows low momentum fluid to be ingested during the suction phase of the DSJ and high momentum fluid to be ejected during the blowing phase. Both phases energize the boundary layer. At high enough  $C_{\mu}$ , the

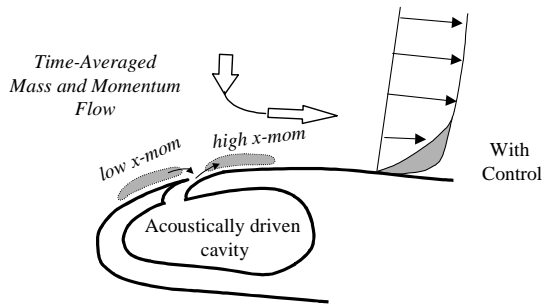


Figure 7. Directed synthetic jet separation control concept

DSJ can suppress separation without the need to operate at an optimum  $F^+$ . The concept and initial validation of the DSJ using a planar diffuser was more fully described in Ref. 24.

### Initial Feasibility Demonstrations

A preliminary effort to evaluate dynamic forcing at full-scale blade conditions was made at UTRC in 1996, as part of an internally-funded effort to investigate active rotor and flow control techniques. A near full scale blade section was modified to include an air supply and high frequency solenoid valves. The pulsed air was expelled from a series of slots near 6% of chord. This technique succeeded in delaying

separation by  $3^\circ$  in steady flow at  $M=0.2$  and  $Re \sim 2 \times 10^6$ , but was less effective at higher Mach numbers or during unsteady blade pitching motions. It is believed that this was caused by insufficient unsteady momentum coefficients being produced by the solenoid valve system ( $C_{\mu} \sim .0001$ ). This initial system was severely constrained by the less than  $0.7 \text{ in}^2$  cross sectional area available ahead of the blade spar in this model.

The initial application of the DSJ to control airfoil separation was performed in 1998 using a similar airfoil model in a low speed steady flow facility. The limited authority of the speaker-based actuation limited this experiment to  $M \sim 0.1$  and  $Re \sim 5 \times 10^5$ . Figure 8 shows a series of smoke flow visualizations at constant angle of attack ( $\alpha = 24^\circ$ ) and increasing  $C_{\mu}$ . At moderate  $C_{\mu}$  (0.002 to 0.005) the leading region reattaches, at higher  $C_{\mu}$  (0.01 to 0.025) the boundary layer becomes essentially attached, and at extremely high  $C_{\mu}$  (0.04) the boundary layer is overdriven to form a wall jet. This experiment demonstrated how the DSJ could operate as an unsteady excitation device at lower  $C_{\mu}$  and as a separation suppression device at higher  $C_{\mu}$ .

The  $C_{\mu}$  level required for full scale rotor blades remains uncertain. No published experiment has fully duplicated the combined parameters of  $M$ ,  $Re$ , unsteady motion, and airfoil contour. Combining the

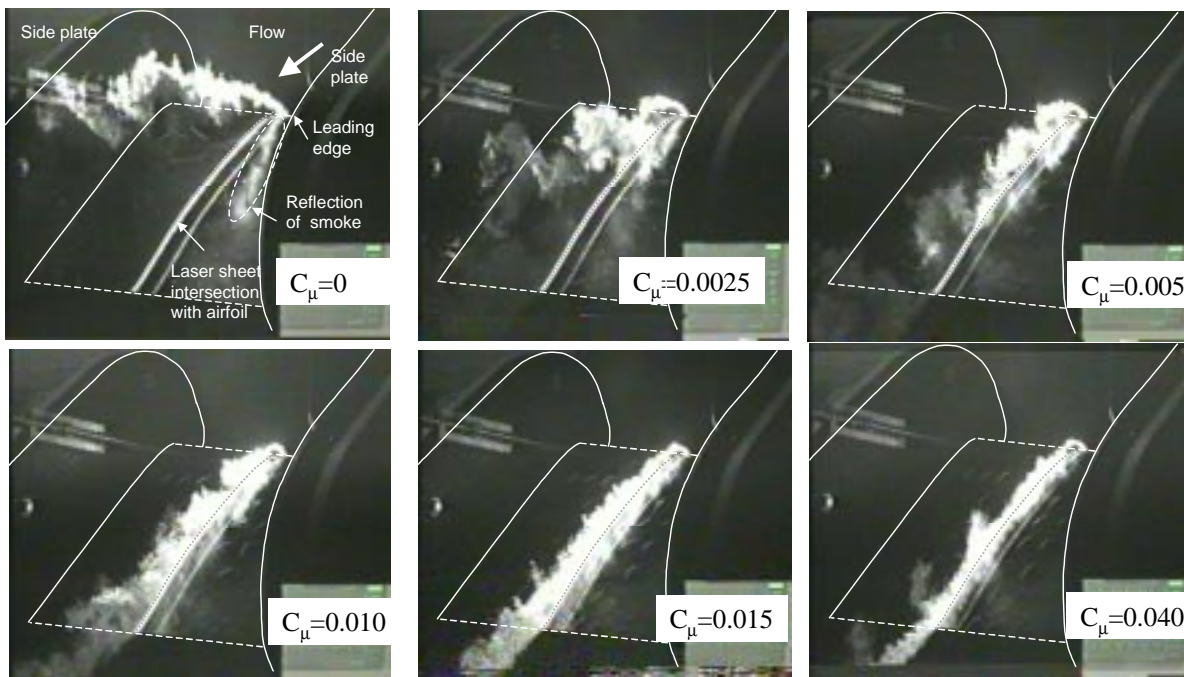


Figure 8. Smoke visualization of DSJ effect on steady airfoil flows  $\alpha = 24^\circ$  (without blockage correction) and  $Re = 1.8 \times 10^5$  (Ref. 24).

results such as Refs. 20, 21, and 24 implies that  $C_{\mu} \sim 0.0001$  is ineffective,  $C_{\mu} \sim 0.001-0.002$  may be acceptable, and  $C_{\mu} \sim 0.005-0.01$  should work well. The approach that has been established for the current program are to increase the blade section stall angle by at least  $5^\circ$  and increase  $C_{Lmax}$  by at least 10% using  $C_{\mu} \sim 0.001$  to 0.002.

### Actuation Options

Actuation is the most difficult technical barrier that must be overcome to implement blade stall control for a full scale helicopter. The following parameters were specified to establish requirements for a RBS control system.

- 20 ft radius, 1.5 ft chord main rotor blades
- Retreating blade relative Mach  $\sim 0.3$  to 0.4
- Apply control from  $\sim 40$  to 85% of radius
- Add less than 10% to blade mass
- Must not compromise structural integrity
- Power requirements  $< 1\%$  of available power

This generated the following actuator requirements:

- $F^+ \sim 1$  implies  $f \sim 300\text{Hz}$
- $C_{\mu} \sim 0.001$  implies  $u_{JET} \sim 200$  fps

An actuator screening was performed in phase 1. Candidates included piezoelectric ceramics, fluidics, electromechanical synthetic jet, passive vibration-driven synthetic jet, periodic flow modulation, and plasma actuation, and microfabricated synthetic jets and plasma actuators. Three appeared most promising for rotorcraft separation control: electromechanical synthetic jet, periodic flow modulation, and plasma actuation. They were evaluated in detail and are discussed below.

### Electromechanical Synthetic Jets

The electromechanical devices considered here are restricted to linear motors driven by an electromagnetic interaction. Initially, three motors were considered: moving coil, variable air-gap, and variable reluctance. The moving coil uses the same principal as audio loudspeakers: the force is controlled by an electromagnet coil moving within a stationary permanent magnetic field. In the variable air gap and reluctance motors, the electromagnet coil is stationary. The coil generates a magnetic circuit through an arrangement of ferrous metal wherein part of the arrangement (the armature) is allowed to move. In the variable air gap, the magnetic flux and force are in alignment creating an extremely strong and nonlinear force at small gaps. In the variable reluctance motor the magnetic flux and force motion are perpendicular, yielding a weaker, but linear force. Dynamic models of each type of motor were constructed to assist in the

evaluation. The main advantages of the variable air gap and reluctance motors were in reliability (no oscillating coil leads) and increased power capacity (coil heat generation can be more readily conducted away). These benefits were out-weighed by the moving coil's lighter moving mass, more manageable tolerances, and commercial availability.

To develop practical actuator embodiments, an electro-acoustic model was developed for a DSJ driven by a moving coil. To validate and tune the model, a prototype DSJ actuator was built using a commercially available motor with 2 inch coil diameter (Fig. 9). The photograph shows the assembled unit and some of the individual components. The schematic drawing shows the

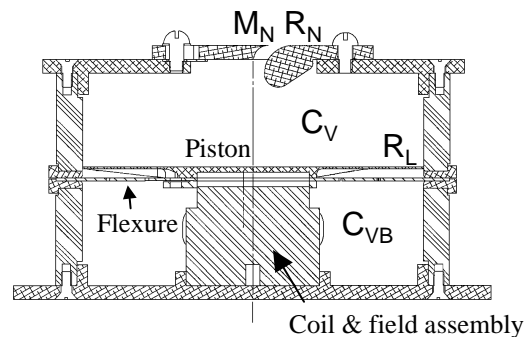
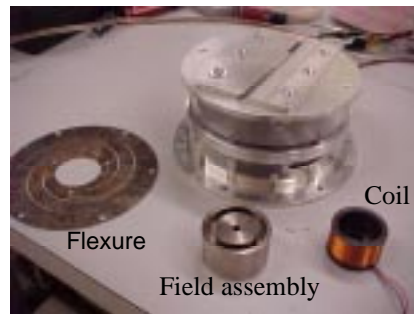


Figure 9. Initial prototype DSJ actuator for bench

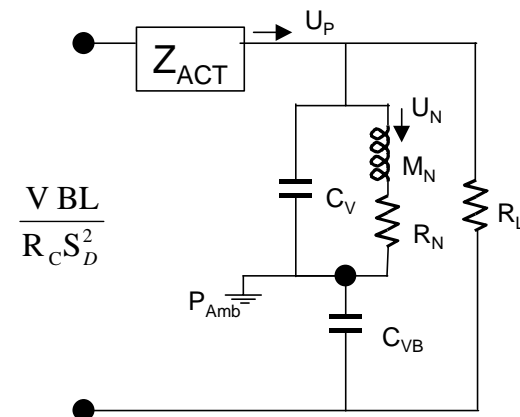


Figure 10. Electro-acoustic model.

assembly and identifies the components associated with the electro-acoustic lumped parameter model of the system shown in Fig. 10.

The “voltage” or potential driving the circuit in Fig. 10 is the acoustic pressure and the “current” is volume velocity equal to the piston volume velocity ( $U_P$ ). The voltage across the coil,  $V$ , has been grouped with motor parameters (magnetic flux, coil length and resistance, and effective area) to form a pressure term. The parameters with subscript “N” refer to neck or slot terms (volume velocity  $U_N = u_{JET} A_N$ , mass  $M_N$ , and resistance,  $R_N$ ). The capacitor elements ( $C_V$ ,  $C_{VB}$ ) in the circuit refer to volumes which act as an acoustic compliance. The circuit model is similar to that described in Ref. 24, with the addition of the acoustic compliance of the sealed backed cavity,  $C_{VB}$ , and the leakage across the piston,  $R_L$ . The model assumes the acoustic mass of the leakage to be negligible.

As given in detail in Ref. 24, the actuator impedance consists of a 2<sup>nd</sup> order system that contains moving mass ( $M_{AT}$ : moving mass of coil, piston, nearby air, and flexure), compliance ( $C_{AS}$ : flexure), and resistance ( $R_{AS}$ : e.g. structural, air viscosity, and eddy current losses). This system can be more simply represented by a resonant frequency,  $\omega_0 = 1/\sqrt{C_{AS} M_{AT}}$  and mechanical quality factor,  $Q_M = R_{AS} \omega_0 / M_{AT}$ . As discussed below, a high quality factor is critical for achieving practical actuation.

Swept-sine tests of the coil electrical impedance with various degrees of acoustic loading were used to improve model parameter estimates and validate the model. For example, a “free-air” test without the slot cover and vented back eliminates all the elements in the circuit model with the exception of  $Z_{ACT}$ . With this measurement, the mechanical quality factor of the actuator can be adjusted in the model to fit the data. (Alternatively, a hammer test with an open coil gives the same results). Sequentially adding the slot cover and sealing the back cavity allows tuning of the neck loss coefficients and effective acoustic neck length. Variation of the drive amplitude is needed to adjust the non-linear jet dump coefficients of the neck and piston leakage. The prototype actuator was also instrumental in identifying and mitigating unexpected loss mechanisms such as eddy currents in the coil former tube.

The efficiency, defined as the acoustic power converted to useful fluid power ( $U_N^2 R_N$ ) divided by the actuator input power, is the primary metric being maximized within the installation constraints. Exercising the model over a range of parameters has been useful for determining several design criteria. For example, aligning the design frequency to the

mass-spring actuator resonance yields the highest efficiency. Matching the Helmholtz mode (neck/cavity) with the mass-spring mode widens the peak bandwidth but does not improve maximum efficiency, and results in an impractical cavity volume. Piston leakage, particularly when the back cavity is sealed, results in large loss in efficiency. Minimizing moving mass while maximizing mechanical quality factor and motor constant ( $BL/R_C^{1/2}$ ), provides the highest efficiency. It is also very important for a given actuator and slot to size the piston correctly in order to provide the best impedance match between the coil and the acoustic load (discussed below).

Once a moving coil motor has been selected for the application, based on the maximum motor constant that fits within space constraints and has minimum coil mass, a criterion is needed to maximize the power output. This criterion is illustrated in Figure 11. The moving coil design point is at the intersection of the force limit (dictated by the thermal dissipation limit so as not to melt the coil) and stroke limit (set by the length of coil winding) where the power (product of coil force and coil velocity) is maximized. Since some of the coil force is used to overcome mechanical and neck losses, the actual DSJ design point is below this point (at the stroke limit for reasonable losses). Since the neck velocity is specified by the design  $C_{\mu}$ , the piston area is given by  $u_N A_N / u_C$ . Hence, the available force given at the DSJ design point in Fig. 11 determines the length of slot which can be optimally driven by the motor. This process is essentially impedance matching the motor to the acoustic load.

To illustrate the importance of mechanical quality factor for practical full scale frequencies and moving mass, the above optimization process was evaluated for a BEI-LA13-12-000A (14 gram coil), moving a 10 gram piston, operating at 225 Hz, slot width of 2.5 mm, and additional jet dump neck losses of 50%

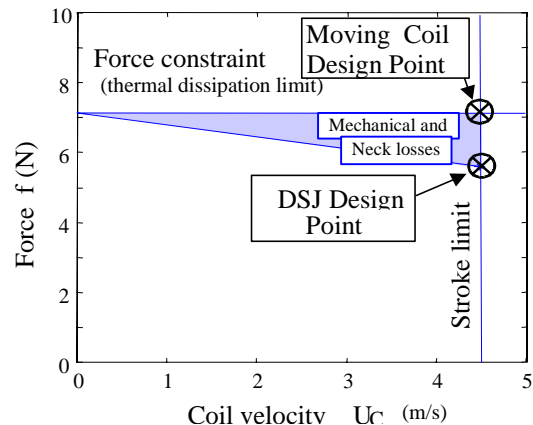


Figure 11. Moving coil actuator optimization

( $K_D=1.5$ ) over a range of mechanical quality factors. The results are shown in Fig. 12 in term of fractions of power consumption versus  $Q_M$ . The figure shows that below  $Q_M = 15$ , mechanical and coil losses dominate, limiting efficiency to 20% or less. In order to achieve efficiencies above 30%, a mechanical quality factor of 50 or more is needed. This is equivalent to a system with 1% or lower damping.

Figure 13 shows a preliminary design for a full

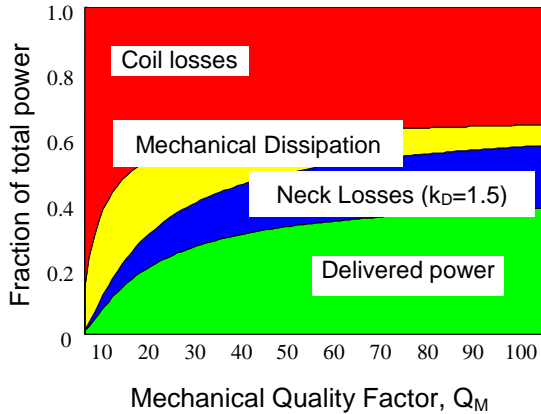


Figure 12. Effect of damping on actuator efficiency

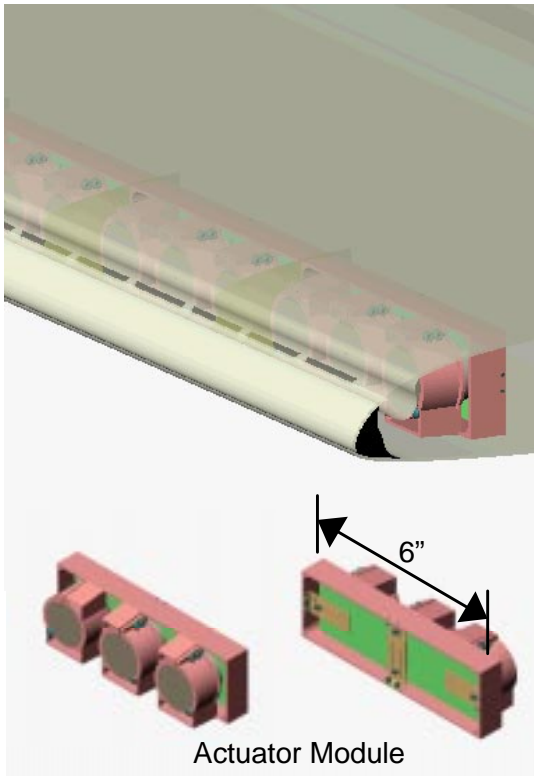


Figure 13. Preliminary design of electromechanical actuator for wind tunnel model.

scale RBS actuator for wind tunnel testing, It uses a BEI-LA13-12-000A motor designed for a frequency of 225 Hz and jet velocity amplitude of 218 f/s ( $F^+ = 1$  and  $C_{\mu} = 0.001$  for the 2 foot chord wind tunnel model). The motors are grouped in packs of three driving one rectangular piston. The actuator modules have sealed back cavities to take advantage of the added stiffness to reduce the required flexure stiffness. Each module is sealed from the neighboring modules on the front, so that both in-phase actuation and actuation with a spanwise alternation of phase can be applied. If alternating phase actuation provides effective stall control, it would enable the use of other actuation arrangements such as rotary motors.

### Periodic Flow Modulation

An alternative to the synthetic jet for generating unsteady  $C_{\mu}$  is modulating net blowing produced by an air source. The modulation actuator can be relatively simple, providing increased reliability at reduced weight and complexity. The use of a steady air supply modulated by a valve in the rotor blade makes a very simple and compact design. A conceptual rotary valve design (Fig. 14) was developed based on two concentric cylinders with slots; the inner cylinder rotating to align these slots for flow out of the valve.

While the number of slots in the rotating cylinder controls the RPM required to obtain a given frequency, the size of the slots controls the airflow and pressure drop. A nominal design compatible with the rotor blade internal dimensions and  $C_{\mu}$  flow requirements has four slots in the rotating element which spins at 4500 rpm to deliver 0.21 lb/hr/blade-ft of air at 300 Hz. This requires an inlet pressure of 2 psid to meet the flow requirements. The power requirement to overcome friction was estimated to be on the order of 0.005 W suggesting that the valve

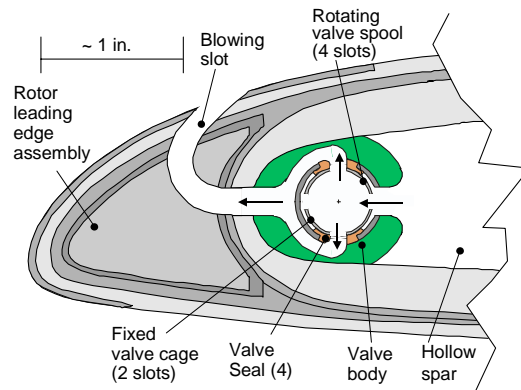


Figure 14. Implementation of a cylindrical rotating valve for periodic bleed air modulation.

could be operated by the equivalent of a common hand-held air motor and powered by the air used for the blowing process. Furthermore, this level of power was much less than the flow power and could be neglected in that analysis.

Engine bleed air was used as the air source in this analysis. It is readily available with no additional equipment required other than plumbing to deliver the compressed air to the rotor blade. However, with only 2 psid required at the rotating cylinder, most of the compression work that has been done by the engine on bleed air (at a nominal 59 psig) is lost in an irreversible expansion. Use of an ejector reduces the bleed airflow requirements and recovers much of the bleed momentum by entraining ambient airflow. However, this process increases the overall efficiency by only about 50%. It should be noted that the use of a low-pressure air source to overcome this problem introduces difficulties of its own; in addition to the added hardware, the large ducting required to deliver the air would be impractical in this application.

Since flow modulation produces only positive velocities, while a synthetic jet produces both positive and negative velocities, higher flow power is required, as shown in Fig. 15. These losses, combined with the inefficiencies of using a high pressure air source result in power requirements ~6-8 times greater than those of a synthetic jet to get the same level of flow modulation for the retreating blade stall application.

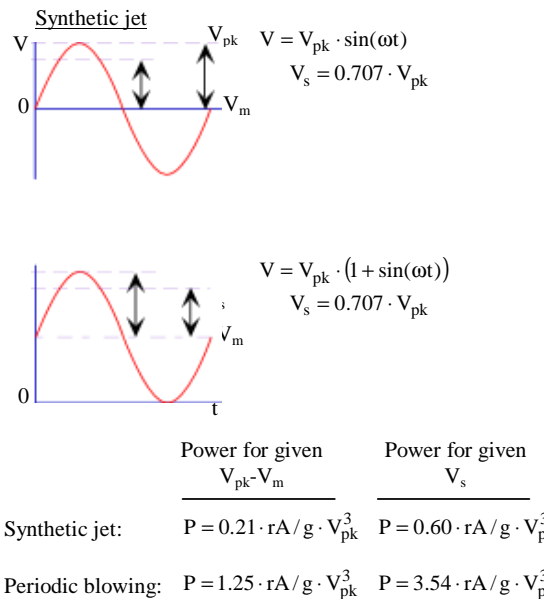


Figure 15. The higher velocity peak associated with periodic blowing requires 6 times the power consumption to generate the same level of flow modulation.

Therefore periodic flow modulation was dropped from further consideration for the RBS application.

### Plasma Actuation

Plasma actuation provides a third actuation path that avoids the mechanical complexity of electromechanical or flow modulation actuators. An extensive effort has been made on the development of actuators which are based on the concept of producing a plasma in a localized region to generate unsteady vortical disturbances. The plasma is produced over electrodes located on a surface, and used to excite a boundary layer or separated shear layer. This type of actuator has been used to excite instability modes in Mach 3.5 laminar boundary layers (Refs. 25-26), and to excite shear layers in incompressible to transonic Mach number jets. As part of the current MAFC program, plasma actuators were evaluated for the RBS application, and demonstrated the potential for producing the required flow velocities. The advantages of the plasma actuators are (1) that they are fully electronic, with no moving parts which can fatigue or limit the frequency band width, (2) they have a high energy density, and (3) they are fully scalable in size, with MEMS scales providing some advantages in their operation.

The plasma flow-actuator concept is illustrated in Fig. 16. For this, an AC voltage is supplied to pair of electrodes. The electrodes are separated by a

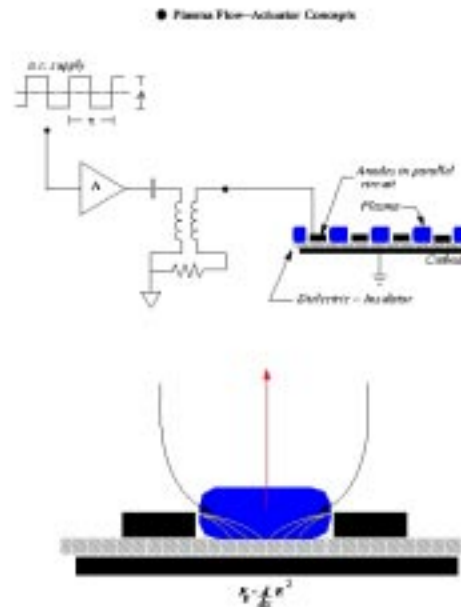


Figure 16. Plasma flow actuator concept.

dielectric-insulator material (Ref. 27). In our first application (Ref. 25), an air gap was used between the electrodes. Presently, we use materials which have better properties than air. When the AC potential across the electrodes exceeds a threshold value (inversely proportional to the electrode spacing and a function of the dielectric properties) the air forms a plasma in the region of highest current flux gradients. The plasma produces a body force on the ambient air,  $F_B \propto \nabla E^2$ . This amounts to a pressure gradient region which induces a flow towards the plasma. The no-penetration boundary condition at the wall results in a secondary flow away from the wall, which is represented in the bottom part of Fig. 16. With electrodes which are aligned with the flow direction, the secondary motion would result in counter-rotating streamwise vortices.

The magnitude of a mean flow component produced by plasma actuators, or the magnitude of unsteady disturbances, can be greatly enhanced by phase-shifting the AC input to an array of neighbor electrodes. This has been done successfully, demonstrating the ability of these actuators to produce high amplitude, alternating velocities at the wall. We envision plasma actuators to be used as a "driver" for synthetic tangential jets in the separation control application. This actuation technology is being developed further and will be applied during the validation experiment described below.

One of the features of plasma actuators that could limit performance is the high voltages required to operate the device. This arises due to the need to develop high electric field strength across the dielectric. One means to lower this voltage is to bring the anode and cathode closer together by using thinner dielectric layers. In an attempt to explore this possibility, a plasma actuator has been fabricated using MEMS technologies (Ref. 28). The device, shown in Fig. 17 is comprised of two series of interdigitated gold electrodes separated by a thin (1 micron) layer of polyamide (Kapton). The device was fabricated, for convenience, on a silicon substrate, although any substrate might be used. The polyamide film serves to dielectrically isolate the two electrodes which are then excited with a high frequency AC signal to create the glow discharge, as described earlier. The device, as shown here, is purely for exploratory purposes and was not tested for any flow control capabilities. It does, however, have some attractive features, primarily that the voltage required to achieve breakdown of the air is somewhat lower than in the "conventional" devices described above. Coupled to this is the need to modulate the driving voltage at a higher frequency than the O(1kHz)

required in the conventional devices. Preliminary tests of the MEMS plasma actuator indicate that they do generate a plasma (visible to the eye) and that the approximate scaling of voltage and frequency is as predicted. However, more detailed experiments need to be conducted before a complete understanding of the device operation and potential benefits is achieved.

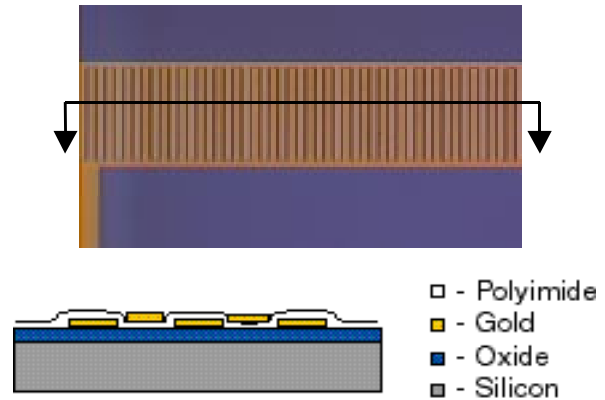


Figure 17. Optical micrograph and schematic cross section of MEMS fabricated plasma discharge actuator.

### Airfoil-Actuator Computations

Unsteady Navier Stokes simulations are being used to evaluate separation control performance at full scale conditions and aid in the design of the actuation system. An initial series of computations have been made for a ramping airfoil with an internal DSJ exiting on the upper surface. The airfoil used in these calculations was the Sikorsky SC2110 airfoil, a modern design which emphasizes improved stall characteristics. The CFL3D Navier-Stokes analysis was used. CFL3D had been used previously at UTRC to predict steady stall enhancement using steady blowing. The Baldwin-Barth turbulence model was used, since it has provided good agreement with experiment in the prediction of the stall onset on full scale blade sections. In addition to the external flow, the flows inside the slot and the plenum were modeled. The objective is to improve the effectiveness of the slot and plenum geometries. The grid near the vicinity of the slot and plenum is shown in Fig. 18. The eight-block grid consisted of 40,083 grid points. An unsteady boundary condition was implemented at the wall in the plenum that represents the DSJ piston. The velocity normal to the wall oscillated by a specified amplitude and frequency to simulate the oscillating wall. The calculations shown here are at  $M=0.1$ ,  $Re=900,000$ .

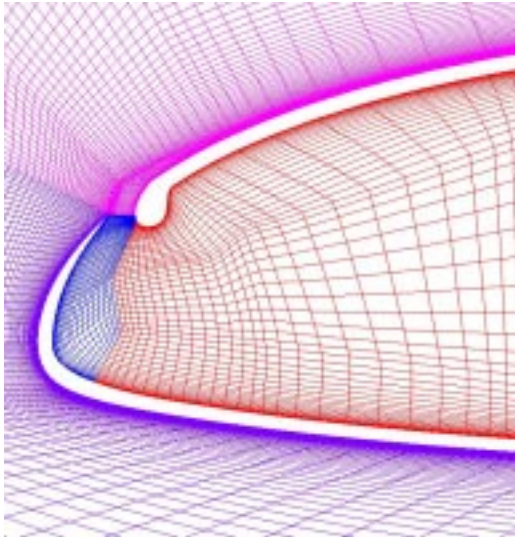


Figure 18. Computational grid in the vicinity of the DSJ slot and plenum.

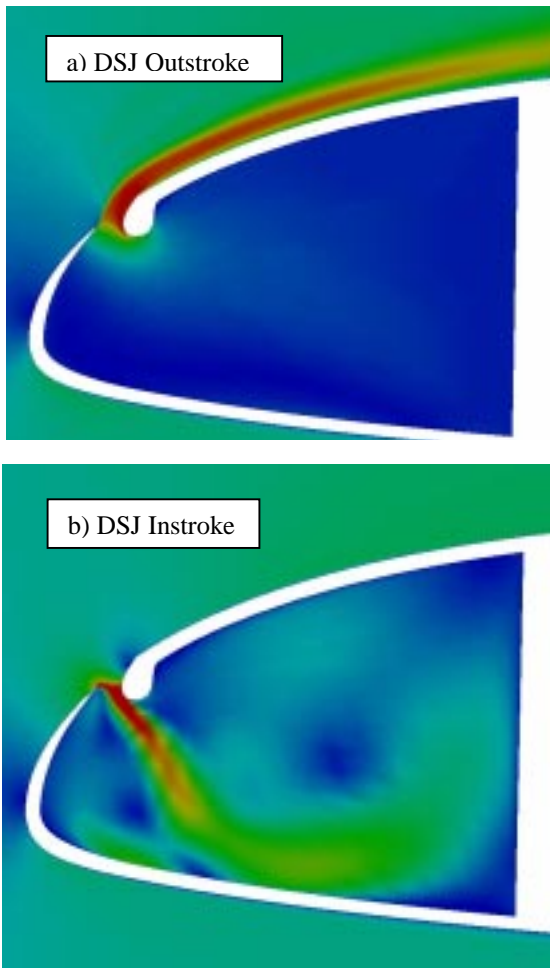


Figure 19. Velocity magnitude contours during the out-stroke(a) and in-stroke(b) of the DSJ

At a low angle of attack, velocity magnitude contours are shown in Figs. 19a and b during the outstroke and instroke of the DSJ. During the instroke, significant losses occur when the jet dumps into the plenum. The CFD analysis is being used to guide improvements in the internal geometry.

Figure 20 shows steady state computational and experimental results for no blowing, and computational results for steady and unsteady jet blowing. The improvement in peak lift coefficient is dramatic for the unsteady jet case with  $C_{\mu} = 1.5\%$  and  $F^+ = 1.0$ . For a ramping airfoil (constant rate increase in pitch at a rate  $A=0.005$ ) the unsteady effects of the pitching motion provide a significant increase in the lift enhancement relative to steady flow. The unsteady lift coefficient histories versus angle of attack are shown in Fig. 21. This figure includes the no blowing case and unsteady blowing cases with the DSJ exit at two different locations:  $x/c = 0.015$  and  $0.064$ . For these calculations,  $C_{\mu}=2\%$ . The peak lift coefficient has a modest increase of 20% with the DSJ located at

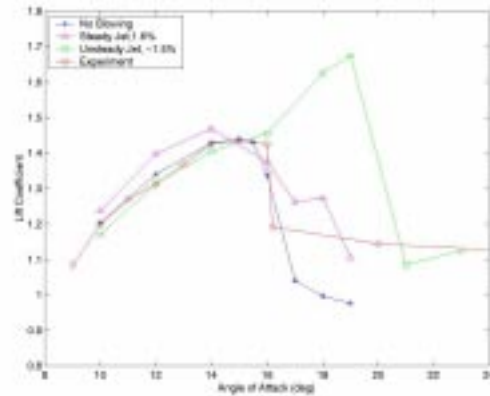


Figure 20.  $C_L$  versus angle of attack for steady SC2110 airfoil. Comparison of steady and unsteady blowing.

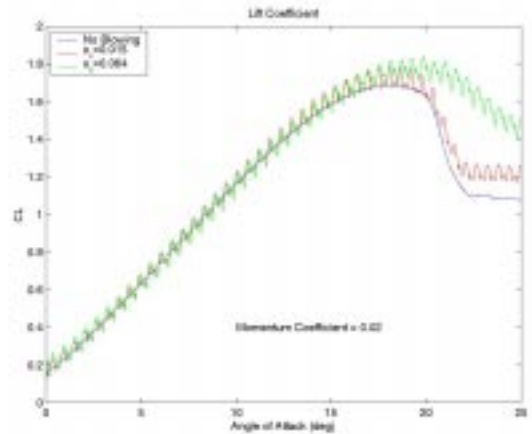


Figure 21. Unsteady  $C_L$  for ramping SC2110 airfoil, effect of DSJ location for  $C_{\mu}=2\%$ .

6.4% chord. Even though the gain in  $CL_{max}$  is not huge, the stall is still significantly softer, which should imply a significant increase in the blade stall boundary.

Analysis of variations in the slot/plenum geometry, the blowing frequency and the slot location are underway to determine the most effective design. These calculations are being done at more representative full scale conditions. It is important to note that the SC2110 airfoil was designed for stall, and thus appears better behaved than the SSC-A09 airfoil used in Refs 7,8, and 11. The stall is softer for the SC2110 than it is for the SSC-A09, which is thinner and has a sharper leading edge. This may limit the gains available from the DSJ. However, use of thicker airfoils such as the SC2110 compromises the high Mach number performance. It may therefore be desirable to apply the DSJ to a thinner airfoil to achieve good stall behavior without compromising the higher Mach number performance.

### Controllers and Sensors

Two modes of operation will be considered: open-loop control and closed-loop control. The closed loop mode has the potential of using less power and delivering more performance than the open loop mode at the expense of requiring separation sensors and logic that is more complex. This tradeoff will be studied in order to obtain the best solution to the problem.

#### Open loop control mode

The simplest control mode is to activate the actuator array during the flight conditions in which separation is known to exist. This control mode requires a schedule that determines the activation/deactivation times based on the flight condition. The control architecture for this mode is simple since no sensors that detect flow separation are required. Despite its simplicity, there are some disadvantages with this approach. In particular, off-line analysis (based on models or heuristics) is required to determine the flight conditions in which separation takes place. Any flight condition in which the prediction of separation is incorrect will yield a sub-optimal system---either the array will be activated when it is not necessary (a power loss) or it will not function when required (a performance loss).

#### Closed loop control mode

A more elaborate control mode is to activate/de-activate the actuator array using sensors that detect flow separation. Pressure or surface shear sensors would be used to detect flow separation. The combination of hot film shear sensors and pressure sensors has been shown to provide good definition of

the development of unsteady transition and separation (Refs. 8-10). To implement this approach a suitable separation precursor signal needs to be constructed from the sensor information. A control law (or logic) that decides the activation/de-activation times based on the precursor signal will be determined. Potentially, this control mode would require less power and yield better performance, than the open loop mode. However, the stability of the overall system is no longer guaranteed. The issues to be addressed in this mode are sensor selection and location, the generation of suitable precursors, the control law, and the stability analysis of the configuration.

The control parameters that affect the overall system behavior include activation and deactivation times (or azimuth angles), forcing frequency, and forcing amplitude. These parameters can be varied on-line to continuously optimize the system performance. Peak-seeking algorithms have been demonstrated for other applications (Ref. 29), and in some low speed proof of concept separation control experiments. These algorithms rely only on measurement of an overall performance variable, and slowly conduct a gradient search over parameter space for the best solution. For current algorithms, the algorithm time constant must be slower than the dynamics (here around 200-300 Hz) to average out their effects, and faster than any maneuver time constants (here, less than 5 Hz) that affect the optimum solution.

#### Stall sensing

Alternatives for sensing flow separation and blade stall include local pressure and shear (heat transfer), strain, and vibration. Strain and vibration sensors on the blade or on the aircraft should be able to readily detect stall onset, but the indications will likely occur too late, after significant dynamic stall. Pressure and shear sensors on the blade surface may be more able to detect precursors to separation or mild stall events in time for the control system to be activated to prevent serious stall. Figure 22 shows typical surface pressure traces at several chordwise ( $x/c$ ) stations during dynamic stall at full scale (Ref. 7-8). Two possible stall indicators are called out. The first is a relatively high frequency oscillation that is often observed prior to separation for  $M > 0.3$ , when there is local supersonic flow near the leading edge. While timely, this indicator has small amplitude and may be hard to distinguish. The second indicator is the rapid increase in the suction (negative) pressure coefficient that occurs while the stall vorticity is collecting. This indicator would be easier to detect by comparing the local pressure to a predetermined function of local

Mach number (derived from radius, rotor RPM, and flight speed).

Surface shear or heat transfer sensors are also able to indicate stall events. Figure 23 shows pressure and hot film gage results for several stall events on an

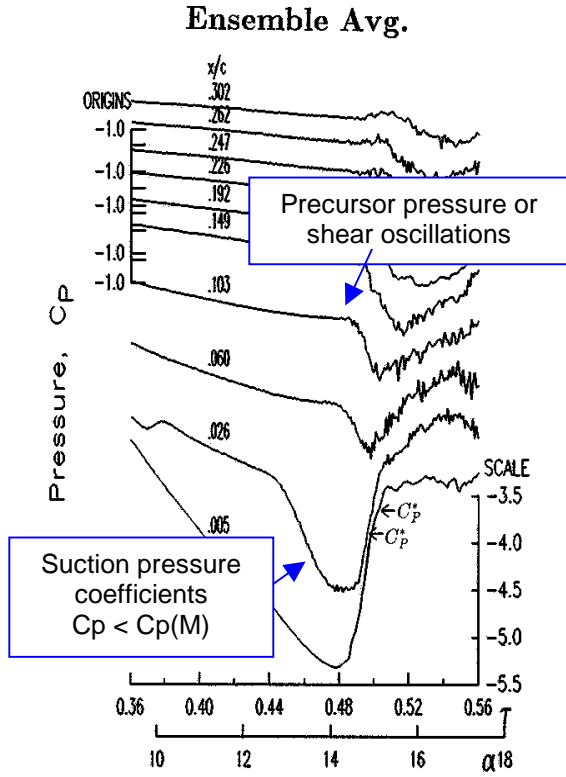


Figure 22. Dynamic stall pressure indicators. Curves show pressure time histories at several chordwise stations during a stall event on an a pitching airfoil

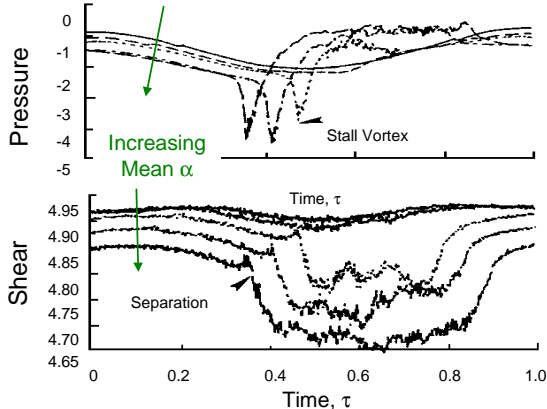


Figure 23. Pressure and shear indicators. Curves show time histories for several stall events on an airfoil at increasing mean angle of attack

oscillating airfoil at increasing mean angle of attack. Both the shear and pressure sensors provide large identifiable changes at stall.

### RBS Control Benefits Analysis

The impact of RBS control on conventional rotor sustained lift limitations is shown in Fig. 24 as rotor thrust versus forward airspeed for baseline and enhanced. The figure normalizes all rotor thrusts by that of the baseline rotor at a minimum power airspeed. Enhanced rotor performance from a blade flow separation control system is incrementally shown for two moderate levels of improvement. The first increment represents a 5 degree increase in the stall angle of attack. The second increment adds an additional 10% increase in  $C_{Lmax}$ . At a constant airspeed, the enhanced design rotor thrust limit is increased by about 12% and this remains relatively unchanged across the spectrum of airspeeds. At a constant thrust, the enhanced design rotor speed limit is increased by about 40 knots at high airspeed and by more at low speed. In Fig. 24, the enhanced rotor system benefit is extended to hover. While rotor stall does not normally limit aircraft system hover capability (where power/torque available usually does), an RBS control system would provide distinct benefits during recovery maneuvers following an engine failure in hover, where rotor limits do play an important role. A multitude of rotorcraft benefits from an RBS control system could exist that would enhance performance, mission effectiveness, maneuverability and survivability.

Aircraft mission effectiveness is enhanced by gains in performance. Payload, range and endurance improvements will result from increases in rotor thrust

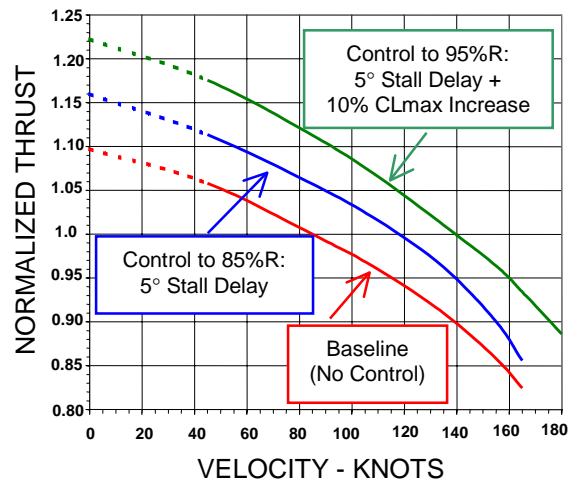


Figure 24. Rotor stall boundary (maximum thrust vs. velocity) curves for baseline and two levels of RBS Control.

margin. Utility helicopters are typically used to transport payload (cargo and/or troops) from one location to another. A normalized H-60 payload versus range chart is shown in Fig. 25 to illustrate this mission. A 23% increase in payload would result from a 12% thrust margin increase, assuming operating weight limitations are increased accordingly. Defense aircraft are often required to perform specific operations at a remote location (radius point) prior to its return flight. This scenario is depicted in Fig. 26 in the form of H-60 on-station endurance versus radius of action. Endurance and range enhancements are made possible by using the additional thrust margin to increase the fuel load at take off where weight limitations would otherwise restrict fuel. Another mission effectiveness scenario where RBS control benefits could be profound is that of deployment. Helicopter ferry missions require auxiliary fuel installations for extended range. These configurations often result in high operating weights requiring maneuverability limits to be imposed. Flight altitudes restrictions also result when high weights encroach on rotor limits. Extended range missions would benefit significantly from an RBS control system, not only in the form of improved rotor efficiency and its associated range, but also from reduced flight times made possible by higher flight speeds. For the examples analyzed, rotor efficiency benefits were neglected in the calculations at increased weights. Weight and power requirements of an RBS control system were also not included for these cases.

Maneuverability will also significantly improve as a result of the increased sustained rotor thrust margins shown in Fig. 24. Nap of the earth (NOE) flight is dominated by low speed masking maneuvers and quick accelerations and decelerations.

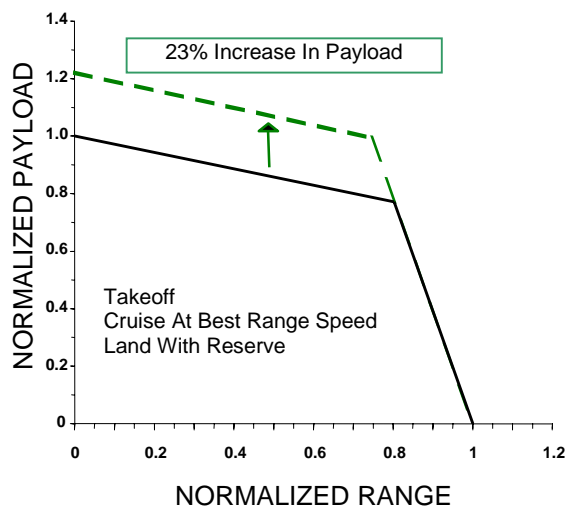


Figure 25. Normalized utility mission payload capability increase created by RBS control system.

Conversely, air-to air combat requires high speed capability and the ability to perform evasive maneuvers, such as pull-ups and high speed decelerating turns. Contour flight requires steady turn rate capability at moderate and high speeds. An RBS control system that improves speed capability and provides a 12% increase in sustained rotor thrust will likely increase turn rates by as much as 30%, increase maximum load factor by up to 0.5g and increase bank angle limitations by 30 degrees. Gains of these magnitudes will dramatically enhance combat survivability.

### Integration

Integration issues are significant for RBS control. Existing blades are fabricated with a hollow composite or titanium structural spar and a light weight honeycomb trailing edge pocket, surrounded by a fiberglass skin. The region ahead of the spar contains counterweights, erosion protection layers, and, if required, deicing systems. The stall control system must either be located in the limited area ahead of the spar or located inside the spar with a fluid or mechanical passageway through the spar. In either case, a significant effort will be needed to avoid compromising spar structural integrity.

Rotor blade control systems must meet severe specifications including vibration, temperature, durability, weight, size, and power required. They must survive the high centrifugal loads (400 g at mid span), vibratory loads, and environmental conditions such as precipitation, particle erosion. Fixed to rotating frame power and information transfer systems must be incorporated.

The primary cost and reliability drivers will be

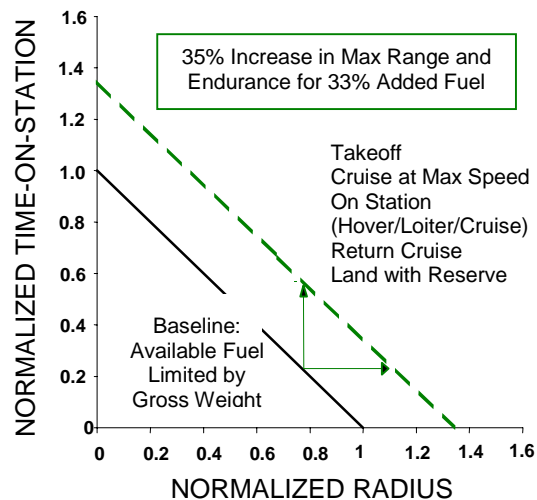


Figure 26. Normalized mission range and endurance enhancement created by RBS control system.

added overall system complexity, which may increase design, fabrication, and maintenance requirements.

### Large Scale Validation Experiment

The most significant issues that must be addressed in order to determine the feasibility of applying flow control to improve rotor blade retreating blade stall characteristics are

1. what unsteady momentum coefficient amplitudes and frequencies are sufficient to achieve significant improvements at realistic conditions?
2. can actuation systems be developed to provide this momentum coefficient within the size, mass and power constraints of a rotor blade?
3. can this system be integrated within a rotor blade and adapted to survive and be maintained in its centrifugal load, vibratory load, and thermal environment?

As a first step, a large scale validation experiment is being developed to answer questions 1 and 2. The experiment will be performed on a full scale ( $M = 0.3$  to  $0.4$ ,  $Re = 3-5 \times 10^6$ ), two dimensional blade section model that can be oscillated at the appropriate frequencies ( $f \sim 4-6$  Hz,  $k = 0.05$  to  $0.15$ ) and amplitudes ( $\pm 10^\circ$ ) at mean angle of  $0$  to  $20$  deg). Figure 27 shows a drawing of the 24 inch chord, 33 inch span blade section model. The airfoil section will be the SC2110, which is used on the inboard sections of new Sikorsky rotor designs.

The experiment will be conducted in a two dimensional channel (TDC) mounted in the 8' octagonal test section of the UTRC Main Wind Tunnel, as shown in Fig. 28. This section is capable of maximum Mach numbers up to  $0.75-0.8$ , providing the capability of not only validating the separation control system under retreating blade conditions, but also of determining any impact on section drag under advancing blade conditions ( $M = 0.7$  to  $0.8$ ).

Unsteady pressure sensors will determine chordwise pressure distributions, lift, pitching moment, and pressure drag coefficients. Surface shear sensors will determine boundary layer state. Both sensors will be available for closed loop control experiments. A wake rake will measure section drag.

Two actuation approaches will be applied. The first experiment, scheduled for Fall 2000, will use electromechanical synthetic jets located inside the model. This experiment is intended to validate the assumptions of required  $C_{\mu}$ , frequency, and jet exit slot location, and determine how well the actuation system performs. The second experiment, scheduled for mid 2001, will use both improved

electromechanical synthetic jet actuators and plasma actuators. This experiment will demonstrate a more flight representative actuation system, and evaluate open and closed loop control architectures.



Figure 27. Drawing of 2D wind tunnel model blade section, showing DSJ slots.

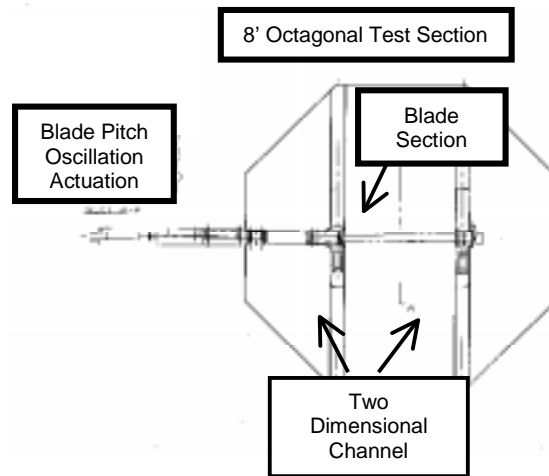


Figure 28. Wind tunnel test section two dimensional channel (TDC) apparatus for full scale pitching blade section validation experiment

### Concluding Remarks

Significant rotorcraft performance benefits can be achieved by implementing retreating blade stall control. Flow control techniques such as synthetic jets and plasma actuation are being developed to effect such control at acceptable levels of mass, power, and complexity. Specific actuation, control, and sensing

embodiments are currently being designed and evaluated. Initial experimental and computational demonstrations have yielded encouraging results. Validation experiments are planned at full scale helicopter rotor blade conditions to demonstrate aerodynamic benefits and actuation and control system performance.

### Acknowledgements

Initial stages of this rotorcraft flow control effort were supported by internal UTRC IR&D programs. Current work is supported by the DARPA MicroAdaptive Flow Control Program (William Scheuren and Richard Wlezian) under U.S. Army Research Office (Thomas Doligalski) Contract DAAG55-98-C-0066.

### References

- Brooks, T.F., and Booth, E.R., "The Effects of Higher harmonic Control on Blade Vortex Interaction Noise and Vibration", *Journal of the American Helicopter Society*, Vol.38, No.3, July 1993.
- Friedman, P.P. and Millot, T.A., "Vibration Reduction in Rotorcraft using Active Control- A Comparison of Various Approaches", AHS Aeromechanics Specialists Conference, San Francisco, CA Jan. 1994.
- Dadone, L., "An Overview of Benefits Possible from the Application of Smart Structure materials to Rotor Blades", ARO 2<sup>nd</sup> Workshop on Smart Structures and Materials, U. Maryland, Sept. 1995.
- Jacklin, Blaas, Teves, and Kube, "Reduction of Helicopter BVI Noise, Vibration, and Power Consumption Through IBC", AHS 51<sup>st</sup> Annual Forum, Ft. Worth TX, May 1995.
- Cheng, R.P., Theodore, C.R., and Celi, R., "Effects of Higher Harmonic Control on Rotor Performance", AHS 56<sup>th</sup> Annual Forum, Virginia Beach VA, May 2000
- Carr, L.W. and Chandrasekhara, M.S., "Compressibility Effects on Dynamic Stall", *Progress in Aerospace Sciences*, Vol. 32, pp. 523-573, 1996
- Lorber, P.F., and Carta, F.O., "Airfoil Dynamic Stall at Constant Pitch Rate and High Reynolds Number," *Journal of Aircraft*, Vol. 25, June 1988, pp. 548-556.
- Lorber, P.F. "Compressibility Effects on the Dynamic Stall of a Three-Dimensional Wing, AIAA Paper 92-0191, 30th Aerospace Sciences Meeting, Jan. 1992.
- Visbal, M.R., "Effect of Compressibility on Dynamic Stall of a Pitching Airfoil", AIAA paper 88-0132, 26<sup>th</sup> Aerospace sciences Meeting, Reno, NV, Jan. 1988
- Grohsmyer, S.P., Ekaterinaris, J., and Platzler, M.F., "Numerical Investigation of the Effect of Leading Edge Geometry on Dynamic Stall of Airfoils", AIAA paper 89-0024. 27<sup>th</sup> Aerospace sciences Meeting, Reno, NV, Jan. 1989
- Patterson, M.T., and Lorber, P.F., "Computational and Experimental Studies of Compressible Dynamic Stall," *Journal of Fluids and Structures*, Vol. 4, 1990, pp. 259-285
- Bousman, W.G., "A Qualitative Examination of Dynamic Stall from Flight Test Data", *Journal of the American Helicopter Society*, Vol. 43, October 1998, pp. 279-295.
- Lorber, P.F., Stauter, R.C., Haas, R.J., Anderson, T.J., Torok, M.J., and Kohlhepp, F.J., "Techniques for Comprehensive Measurement of Model Helicopter Rotor Aerodynamics, 50th Annual Forum of the American Helicopter Society, May 1994.
- Carr, L.W., and McAlister, K., "The Effect of a Leading Edge Slat on the Dynamic Stall of an oscillating Airfoil", AIAA Paper 83-2533, AIAA/AFS Aircraft Design, Systems, and Operations Meeting, Ft. Worth TX, Oct. 1983
- Narramore, J.C., McCroskey, W.J., and Noonan, K.W., "Design and Evaluation of Multi-Element Airfoils for Rotorcraft", AHS 55<sup>th</sup> Annual Forum, Montreal, Quebec, May 1999.
- Yu, Y.H., McAlister, K.W., Tung, C., and Wang, C.M. "Dynamic Stall Control for Advanced Rotorcraft Application", *AIAA Journal*, Vol.33, No. 2, Feb. 1995.
- Karim, M.A. and Achyara, M., "Control of the Dynamic Stall Vortex over a Pitching Airfoil by Leading Edge Suction", AIAA Paper 93-3267, Shear Flow Conference, Orlando FL, July 1993.
- Koga, D.J., Reisenhal, P., and Nagib, H.M. "Control of Separated Flows Using Forced Unsteadiness" Illinois Institute of Technology Fluids & Heat Transfer Report R84-1, 1984
- Katz, Y., Nishri, B., and Wygnanski, I., "The Delay of Turbulent Boundary Layer Separation

- by Oscillatory Active Control," AIAA Paper 89-0975, 1989
20. Seifert, A. and Pack, L.G., "Oscillatory Control of Separation at High Reynolds Numbers", AIAA Paper 98-0214, 36<sup>th</sup> Aerospace sciences Meeting, Jan. 1998
  21. Greenblatt, D., and Wygnanski, I., "Parameters Affecting Dynamic Stall Control by Oscillatory Excitation," AIAA Paper 99-3121, 17<sup>th</sup> Applied Aerodynamics Conference, Norfolk VA, 28 June-1 July 1999.
  22. Ingard, U, "On the Theory and Design of Acoustic Resonators", *Journal of the Acoustical Society of America*, Vol. 25, No. 6, November 1953
  23. Amitay, M., Smith, B.L., and Glezer, A, "Aerodynamic Flow Control Using Synthetic Jet Technology", AIAA 98-0208, January 1998
  24. McCormick, D.C., "Boundary Layer Separation Control with Directed Synthetic Jets." AIAA Paper 2000-0519, 38<sup>th</sup> Aerospace Sciences Meeting, Reno, NV Jan 2000.
  25. Cavalieri, D. "On the Experimental Design for Instability Analysis on a Cone at Mach 3.5 and 6 Using a Corona Discharge Perturbation Method", M.S. Thesis, Illinois Institute of Technology, 1995
  26. Corke, T. C. and Cavalieri, D. "Controlled experiments on instabilities and transition to turbulence in supersonic boundary layers", AIAA Paper 97-1817, 1997.
  27. Massines, F. Rabehi, A., Decomps, P. Gadri, R. Segur, P. and Mayoux, C. "Experimental and theoretical study of a glow discharge at atmospheric pressure controlled by a dielectric barrier", *J. App. Physics*, Vol. 83, No. 6, pp. 2950-2957, 1998.
  28. Bayt, R.L. and Breuer, K.S. Private Communication. 2000
  29. Banaszuk, A., Zhang, Y, Jacobson, C.A., "Adaptive Control of Combustion Instability Using Extremum-Seeking", 2000 American Control Conference, June 2000.